CERN – SL DIVISION

kickermodel.tex

CERN-SL-2000-004 AP

Some Simplified Models of Ferrite Kicker Magnet for Calculation of Longitudinal Coupling Impedance

H. Tsutsui

Abstract

Four simplified models of a ferrite kicker magnet are presented to calculate its longitudinal coupling impedance. Also, the impedance measured by coaxial wire method is estimated and compared with the analytical calculation. The model is evaluated with HFSS simulation.

Geneva, Switzerland

January 28, 2000

Contents

1 Introduction

In a synchrotron ring, kickers have large contribution to the longitudinal coupling impedance [1]. In this report, we calculate the longitudinal impedance and the impedance by coaxial wire method with very simplified kicker models, and compare the results with the measurements of the SPS MKE kicker [2].

The first model (Model 1) is discussed in Section 2. This has axially symmetric geometry. Analytical calculation for this model shows much higher impedance than the measurement at 200 MHz. The electromagnetic simulation code HFSS [3] is used to check the calculation.

Next model (Model 2) is discussed in Section 3. The reason why Model 1 gives higher impedance at low frequency may be because there are no metal electrodes in the model. So, we put metal plates both sides and modified the geometry in order to calculate the impedance analytically. Analytical calculation of the impedance shows good agreement with the measurement at low frequency ($\leq$ 200 MHz). But at high frequency ($\geq$ 400 MHz) this model gives higher impedance. Also, the measurement by the coaxial wire method is simulated with HFSS.

Since the Model 2 gives higher impedance at high frequency ($\geq$ 400 MHz), we modified the side metal plates and the ferrite block to more realistic geometry (Model 3) to see the effect of them. The HFSS simulations show that these effects are small for real beam, but the imaginary part of the impedance by the coaxial wire method becomes larger because of a trapped mode around the outer metal plate. This topic is shown in Section 4.

From the comparison of Model 2, Model 3 and the measurement, we thought that some by-passing modes are created in the kicker and they make the real and imaginary parts of the impedance in the measurement small and large. In the SPS MKE kicker, the electromagnetic field at high frequency can easily travel between the ferrite block and the vacuum vessel. So, we input almost real structure of the SPS MKE kicker to the HFSS, and simulated the measurement by the coaxial wire method. The result agrees with the real measurement well. This is shown in Section 5.

From the longitudinal impedances, the power dissipated into the ferrite kicker is calculated in Section 6. The values are compared with the energy consumption measurement done in the SPS.

2 Model 1

The simplest model of a ferrite kicker, consisting of a cylindrical ferrite shell, is shown in Figure 1. We assume the length in axial direction is infinite in this report. Ferrite is at $b < r < d$. There is vacuum

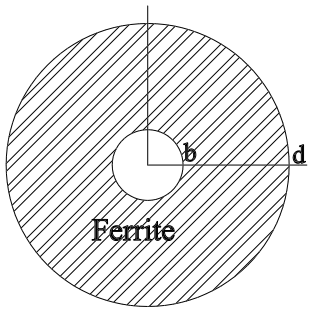

Figure 1: Model 1

inside ($r < b$). The outside ($r > d$) is filled with perfect conductor. The beam passes at $r = 0$.

2.1 Analytical Calculation

The impedance calculation of this model is a simple extension of that of the resistive wall [4]. The axial component of the beam current density (j_z) of angular frequency ω is described as

$$j_z(r,\phi,z) = \frac{I_0}{2\pi r}\exp(j\omega(t-z/c))\delta(r). \tag{1}$$

Throughout this report, we assume the beam has the velocity of light c. Sometimes the exponential term $\exp(j\omega(t-z/c))$ will be omitted below.

This current density create a TEM field:

$$E_r^{(S)} = Z_0 H_\phi^{(S)} = \frac{Z_0 I_0}{2\pi r}, \tag{2}$$

where $Z_0 = c\mu_0 = 377\ \Omega$ is the characteristic impedance in vacuum.

Also a TM0 mode in the vacuum region $r < b$ is excited. Since the wave number in the axial direction k is ω/c, the wave number in the radial direction is zero in the vacuum region. So, the corresponding Bessel functions simply to $J_0(k_r r) \to 1$, $J_1(k_r r) \to k_r r/2$. Thus, the field is

$$\begin{aligned} E_z &= A, \\ E_r &= A\frac{jkr}{2}, \\ Z_0 H_\phi &= A\frac{jkr}{2}. \end{aligned} \tag{3}$$

The field in the ferrite is

$$\begin{aligned} E_z &= (BH_0^{(2)}(k_r r) + CH_0^{(1)}(k_r r)), \\ E_r &= \frac{jk}{k_r}(BH_1^{(2)}(k_r r) + CH_1^{(1)}(k_r r)), \\ Z_0 H_\phi &= \frac{jk\epsilon_r}{k_r}(BH_1^{(2)}(k_r r) + CH_1^{(1)}(k_r r)), \end{aligned} \tag{4}$$

where $k_r = k\sqrt{\epsilon_r\mu_r - 1}$, H is the Hankel function. The relative permittivity ϵ_r is $\epsilon_r' - j\epsilon_r'' + \sigma/(j\omega\epsilon_0)$. The relative permeability μ_r is $\mu_r' - j\mu_r''$.

From the boundary condition at $r = b$ and $r = d$, the following relations are obtained,

$$\begin{aligned} A &= BH_0^{(2)}(k_r b) + CH_0^{(1)}(k_r b), \\ \frac{Z_0 I_0}{2\pi b} + A\frac{jkb}{2} &= (BH_1^{(2)}(k_r b) + CH_1^{(1)}(k_r b))\frac{jk\epsilon_r}{k_r}, \\ BH_0^{(2)}(k_r d) + CH_0^{(1)}(k_r d) &= 0. \end{aligned} \tag{5}$$

The impedance per unit length Z/L is [5]

$$\frac{Z}{L} = -\frac{A}{I_0} = \frac{Z_0}{2\pi b}\frac{j}{\frac{H_0^{(1)}(k_r d)H_1^{(2)}(k_r b) - H_0^{(2)}(k_r d)H_1^{(1)}(k_r b)}{H_0^{(1)}(k_r d)H_0^{(2)}(k_r b) - H_0^{(2)}(k_r d)H_0^{(1)}(k_r b)}\frac{k\epsilon_r}{k_r} - \frac{kb}{2}}. \tag{6}$$

When $d \to \infty$, the Hankel function $H_0^{(1)}(k_r d)$ goes to infinity, and the above equation can be simplified as,

$$\frac{Z}{L} = \frac{Z_0}{2\pi b}\frac{j}{\frac{H_1^{(2)}(k_r b)}{H_0^{(2)}(k_r b)}\frac{k\epsilon_r}{k_r} - \frac{kb}{2}}. \tag{7}$$

In our case, the wave number k_r can be approximated as $k_r \simeq \sqrt{\epsilon_r \mu_r} k \simeq (1-j)\sqrt{\epsilon'_r \mu''_r / 2} k$. If we assume $|k_r b| \geq 1$, the Hankel functions go to $H_1^{(2)}(k_r b)/H_0^{(2)}(k_r b) \simeq j$. With these assumptions, we obtain

$$\frac{Z}{L} \simeq \frac{Z_0}{2\pi b} \frac{1}{\frac{k\epsilon_r}{k_r} + \frac{jkb}{2}} \simeq (1-j)\frac{Z_0}{2\pi b}\sqrt{\frac{\mu''_r}{2\epsilon'_r}} \frac{1}{1 + \frac{1-j}{2}\sqrt{\frac{\mu''_r}{2\epsilon'_r}} kb} \simeq (1-j)\frac{Z_0}{2\pi b}\sqrt{\frac{\mu''_r}{2\epsilon'_r}}. \tag{8}$$

It is interesting to see that this impedance has capacitive component.

Figure 2 shows the relative permeability of 4A4 ferrite [6, 7]. This ferrite is used in the SPS MKE

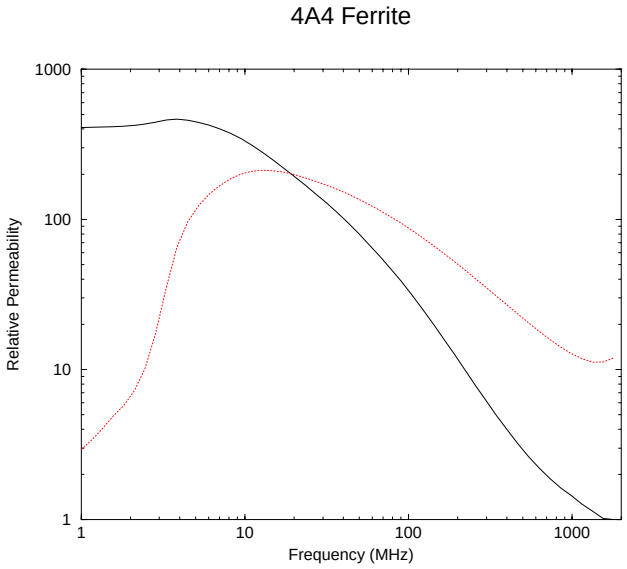

Figure 2: Relative permeability of 4A4 ferrite. The solid and dotted lines show the real and imaginary parts, respectively. Relative permittivity of 4A4 is $\epsilon_r = 12$.

kicker. We assume that the permittivity is $\epsilon'_r = 12$. There is some ambiguity on the value of the conductivity σ [1]. For the sake of the simplicity, we assume $\sigma = 0$.

Figure 3 shows the longitudinal impedance per unit length. From the right graph of Figure 3, we can observe that when the thickness of the ferrite is finite there is a resonance. The resonance condition is $d - b \simeq \lambda/(4\sqrt{|\epsilon_r||\mu_r|})$. From this, the resonant frequency for our case is 30 MHz, which agrees with the graph.

2.2 Simulation with HFSS

The method of the simulation is discussed in [8].

The geometry is shown in Figure 4. We chose the variables as $b = 20$ mm and $d = 80$ mm. The length in axial direction is now finite and equal to 1 m. Since HFSS has some option to assign some currents on planes, we used this to simulate the beam. Current sources of 2 cm length are tiled around the axis. Phase difference between adjacent currents is 2 cm / $\lambda \times 360°$.

Since this geometry has axial symmetry, we used 1/36 model for the simulation. Figure 5 shows the electromagnetic field at 200 MHz.

In this simulation, we put 1 A current source around the axis. Since the model is 1/36, we anticipated that the total current is 36 A. But the excited field is much smaller. This may be due to the boundary condition problem in HFSS. So, we decided to calculate the current on the axis from H_ϕ. To minimize the effect of E_z, we observed H_ϕ at small radius. The left graph shows H_ϕ at $r = 5$ mm. Since the maximum value of H_ϕ is 60 A/m, the current I_0 at the axis is $I_0 \simeq 2\pi r H_\phi = 1.9$ A.

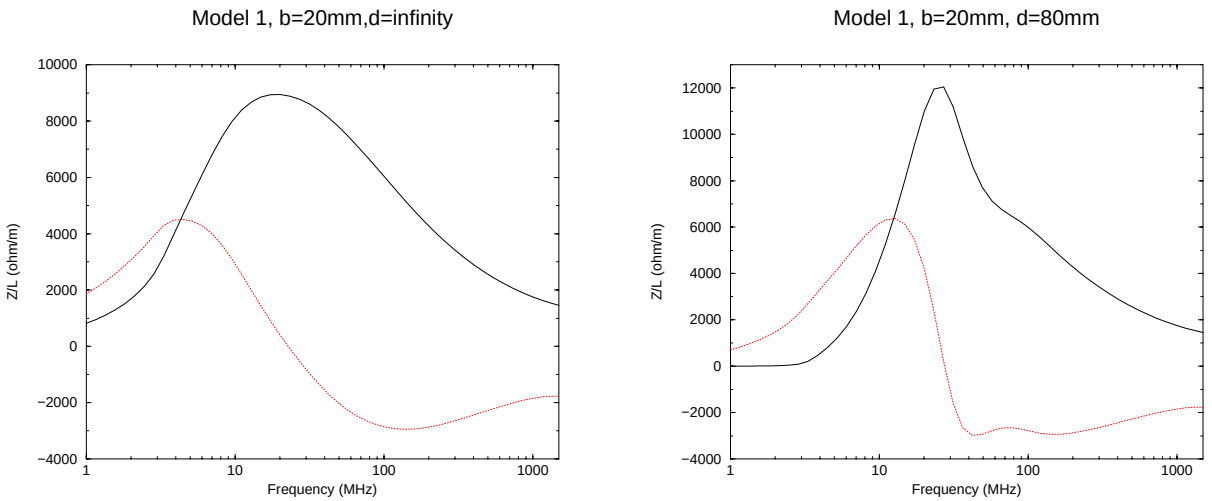

Figure 3: Longitudinal coupling impedance per unit length for Model 1 for infinite (left) and finite (right) ferrite thickness. The solid and dotted lines show the real and imaginary parts, respectively.

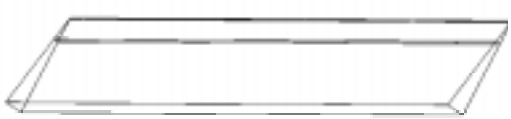

Figure 4: Model 1 geometry used for HFSS: only 1/36 of the structure is simulated.

The right figure shows E_z at $r = 20$ mm. Since in our case E_z is independent of the transverse coordinate in the vacuum, we can use this value to calculate the impedance. One can see $E_z = 9300\angle 145^\circ\ V/m$. Thus the impedance per unit length is $Z/L = -E_z/I_0 = (4100 - j2800)\ \Omega$/m at 200 MHz. At 200 MHz, the measurement [2] gave $\mathrm{Re}(Z_{CW}) = 600\ \Omega$ for the SPS MKE kicker. Since the length of the ferrite is $l = 1.658$ m, the impedance per length is $\mathrm{Re}(Z_{CW}/L) = 360\ \Omega$/m. So, the

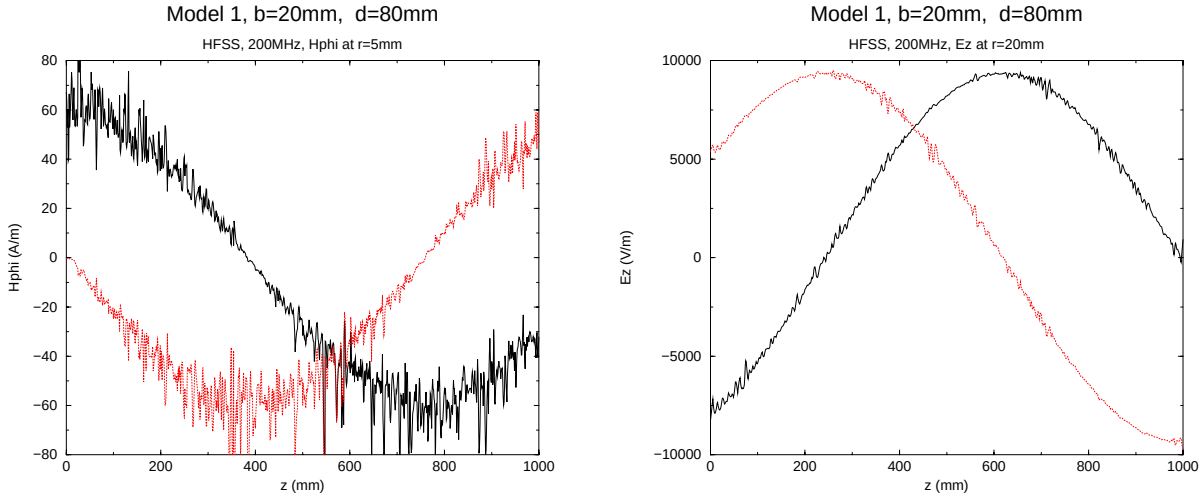

Figure 5: Electromagnetic field along a 1 m long ferrite cylinder corresponding to Model 1 at 200 MHz by HFSS simulation. Solid and dotted lines show the real and imaginary parts, respectively.

result is about 10 times larger.

Figure 6 shows the result of HFSS simulation.

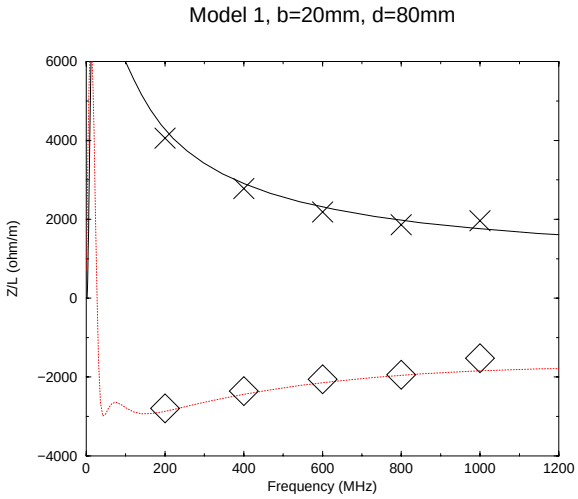

Figure 6: Longitudinal impedance per unit length of Model 1 by HFSS. Cross and diamond symbols show the real and imaginary parts by HFSS simulation. Solid and dotted lines show the real and imaginary parts of the impedances by analytical calculation.

2.3 Coaxial Wire Method

2.3.1 Analytic Calculation

For distributed impedance systems like our ferrite kicker, the following 'Log' formula is used in the coaxial wire measurement [2]:

$$Z_{CW} = -2Z_c \log(S_{21}/S_{21ref}). \tag{9}$$

In this equation, Z_c and S_{21} are the characteristic impedance and the transmission coefficient, respectively. The transmission coefficient S_{21} in our case is $\exp(-\gamma l)$, where γ, l are the attenuation constant and the length of the DUT. The reference transmission coefficient S_{21ref} is $\exp(-j\omega l/c)$. Thus the 'Log' formula becomes

$$\frac{Z_{CW}}{L} = 2Z_c(\gamma - j\omega/c). \tag{10}$$

So, what we have to know to calculate Z_{CW}/L are the characteristic impedance Z_c and the attenuation constant γ.

The characteristic impedance Z_c is given in [2] as,

$$Z_c = \frac{Z_0}{2\pi} \log(b/a), \tag{11}$$

where a is the wire radius. Though we are not sure whether this formula is correct for this case, we will use this because there are no alternatives now.

Next we calculate the attenuation constant. The electromagnetic field in the vacuum region ($a < r < b$) is

$$\begin{aligned} E_z &= (AJ_0(k_1 r) + BN_0(k_1 r)) \exp(j\omega t - \gamma z), \\ E_r &= (AJ_1(k_1 r) + BN_1(k_1 r)) \frac{\gamma}{k_1} \exp(j\omega t - \gamma z), \\ Z_0 H_\phi &= j\frac{k}{\gamma} E_r, \end{aligned} \tag{12}$$

where J and N are the Bessel function and the Neumann function, respectively. The wave number k_1 is $\sqrt{k^2+\gamma^2}$. The electromagnetic field in the ferrite is

$$\begin{aligned} E_z &= (CJ_0(k_2r)+DN_0(k_2r))\exp(j\omega t-\gamma z), \\ E_r &= (CJ_1(k_2r)+DN_1(k_2r))\frac{\gamma}{k_2}\exp(j\omega t-\gamma z), \\ Z_0H_\phi &= j\frac{k\epsilon_r}{\gamma}E_r. \end{aligned} \tag{13}$$

The wave number k_2 is $\sqrt{k^2\epsilon_r\mu_r+\gamma^2}$.

From the boundary conditions at $r=a,b,d$, we obtain

$$\begin{aligned} AJ_0(k_1a)+BN_0(k_1a) &= 0, \\ AJ_0(k_1b)+BN_0(k_1b) &= CJ_0(k_2b)+DN_0(k_2b), \\ (AJ_1(k_1b)+BN_1(k_1b))/k_1 &= \epsilon_r(CJ_1(k_2b)+DN_1(k_2b))/k_2, \\ CJ_0(k_2d)+DN_0(k_2d) &= 0. \end{aligned} \tag{14}$$

The attenuation constant γ can be obtained by solving the above equations for A, B, C, D, and γ.

Figure 7 shows the longitudinal impedance per unit length by the coaxial wire method. It is seen that when the wire radius is 1 mm, $|Z_{CW}/L|$ is smaller than $|Z/L|$. In this case, the characteristic impedance is 180 Ω. When the wire radius is 10^{-100} mm, the characteristic impedance becomes 13700 Ω. In this case, Z_{CW}/L approaches to Z/L.

2.3.2 HFSS

The geometry is shown in Figure 8. The axial length of the ferrite is 1 m. We add two waveguides of 5 cm length, 2 cm radius on both sides, in order to have regular TEM modes at both ports. The radius of the wire is 1 mm. The characteristic impedance Z_c of the coaxial waveguide is $Z_0/(2\pi)\log(20/1)=180\,\Omega$.

For example at 200 MHz, the scattering parameter is $S_{21}=0.00010\angle-329.222^\circ$. Then the impedance is

$$\begin{aligned} \mathrm{Re}(Z_{CW}/L) &= -2Z_c\log 0.00010 = 3309\ \Omega/\mathrm{m}, \\ \mathrm{Im}(Z_{CW}/L) &= -2Z_c(\arg S_{21}+\omega l/c) = 408\ \Omega/\mathrm{m}. \end{aligned} \tag{15}$$

Figure 9 shows the simulated versus analytical longitudinal impedance per unit length by the coaxial wire method.

3 Model 2

Compared with the measurement [2], Model 1 gives much larger impedance at 200 MHz. This may be because we neglected metal electrode plates at the two sides. In the kicker at lower frequency, the electromagnetic field should be strongly deformed so that most of the image current go through the electrode plates. This lowers the impedance at low frequency. So, we added electrodes at both sides in the Model 2, and we deformed the ferrite block in order to calculate the impedance analytically. The model is shown in Figure 10. Ferrite is at $-a<x<a, b<|y|<d$. There is vacuum between two ferrite rectangular blocks ($-a<x<a, -b<y<b$). The outside ($|x|>a$ or $|y|>d$) is filled with perfect conductor. The beam passes at $x=y=0$.

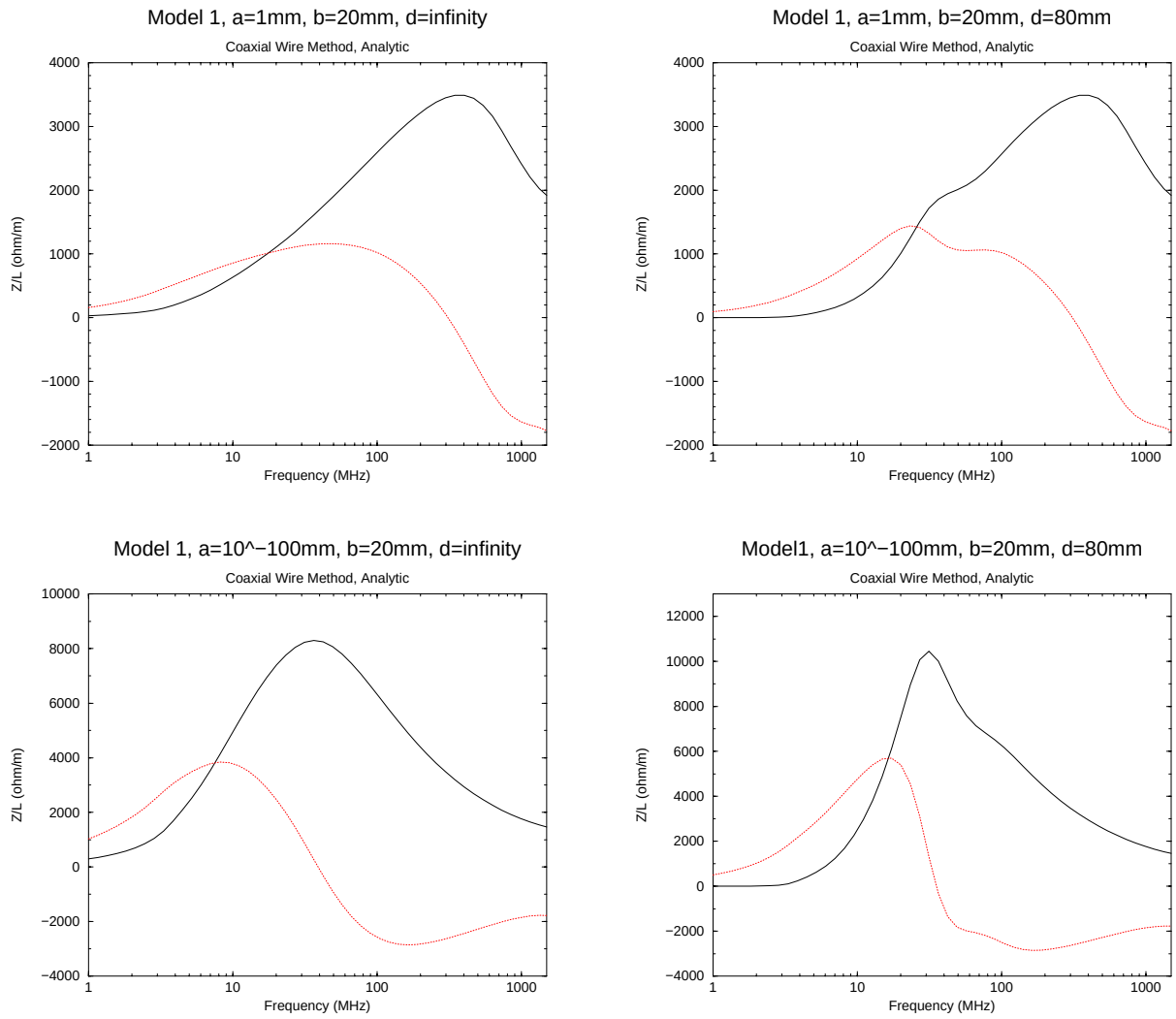

Figure 7: Longitudinal impedance per unit length for Model 1 with coaxial wire method (analytical calculation). The solid and dotted lines show the real and imaginary parts, respectively.

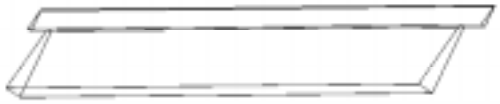

Figure 8: Model 1 geometry with coaxial wire used for HFSS.

3.1 Analytical Calculation

For the source field $(E_r^{(S)}, H_\phi^{(S)})$, we can use Eq. (2). But this field does not satisfy the new boundary conditions at $|x| = a$. Since it is convenient for the field to satisfy the boundary condition at $|x| = a$, we add image current densities at $(x, y) = (2na, 0), n = 0, \pm 1, \pm 2, \cdots$. The modified field becomes

$$
\begin{aligned}
(E_x^{(S)}, E_y^{(S)}) = (Z_0 H_y^{(S)}, -Z_0 H_x^{(S)}) &= \frac{Z_0 I_0}{2\pi} \sum_{n=-\infty}^{\infty} (-1)^n \frac{(x - 2na, y)}{(x - 2na)^2 + y^2} \\
&= \frac{Z_0 I_0}{2a} \frac{(\sin(\pi x/(2a)) \cosh(\pi y/(2a)), \cos(\pi x/(2a)) \sinh(\pi y/(2a)))}{\cosh(\pi y/a) - \cos(\pi x/a)} \qquad (16)
\end{aligned}
$$

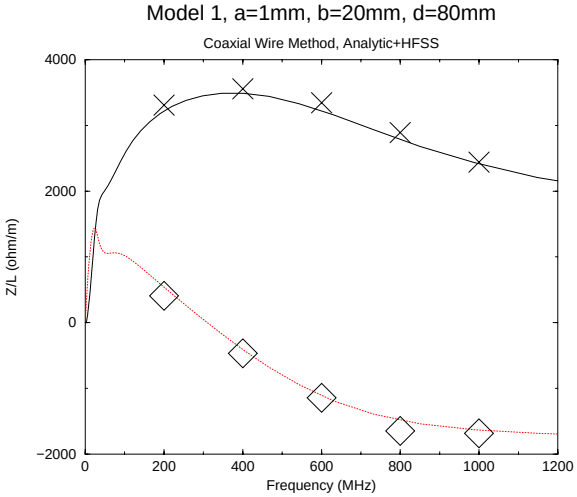

Figure 9: Longitudinal impedance per unit length for Model 1 with coaxial wire method (analytical calculation, HFSS). The solid and dotted lines show the real and imaginary parts by analytical calculation. Cross and diamond symbols represent the real and imaginary parts by HFSS simulation.

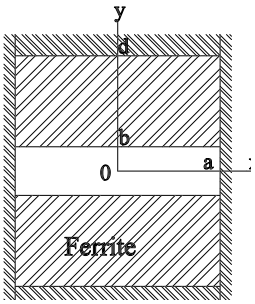

Figure 10: Model 2: cross section for the modified, rectangular geometry. The beam moves along z (out of the page).

There are waveguide modes in the vacuum region:

$$
\begin{aligned}
E_z &= \sum_n (A_n + B_n)\cos(k_{xn}x)\cosh(k_{xn}y), \\
E_x &= \sum_n \frac{jk}{k_{xn}} A_n \sin(k_{xn}x)\cosh(k_{xn}y), \\
E_y &= \sum_n \frac{jk}{k_{xn}} B_n \cos(k_{xn}x)\sinh(k_{xn}y), \\
Z_0 H_z &= \sum_n (A_n + B_n)\sin(k_{xn}x)\sinh(k_{xn}y), \\
Z_0 H_x &= j\sum_n (\frac{k_{xn}}{k} A_n + (\frac{k_{xn}}{k} - \frac{k}{k_{xn}}) B_n)\cos(k_{xn}x)\sinh(k_{xn}y), \\
Z_0 H_y &= j\sum_n ((\frac{k_{xn}}{k} + \frac{k}{k_{xn}}) A_n + \frac{k_{xn}}{k} B_n)\sin(k_{xn}x)\cosh(k_{xn}y),
\end{aligned}
\tag{17}
$$

where $k_{xn} = (2n+1)\pi/(2a), n = 0, 1, 2, \cdots$.

The field in the upper ferrite block is

$$
E_z = \sum_n C_n \cos(k_{xn}x)\sin(k_{yn}(y-d)),
$$

$$
\begin{aligned}
E_x &= \frac{j}{\epsilon_r\mu_r - 1}\sum_n (\frac{k_{xn}}{k}C_n + \mu_r\frac{k_{yn}}{k}D_n)\sin(k_{xn}x)\sin(k_{yn}(y-d)),\\
E_y &= \frac{j}{\epsilon_r\mu_r - 1}\sum_n (\frac{-k_{yn}}{k}C_n + \mu_r\frac{k_{xn}}{k}D_n)\cos(k_{xn}x)\cos(k_{yn}(y-d)),\\
Z_0H_z &= \sum_n D_n\sin(k_{xn}x)\cos(k_{yn}(y-d)),\\
Z_0H_x &= \frac{j}{\epsilon_r\mu_r - 1}\sum_n (\epsilon_r\frac{k_{yn}}{k}C_n - \frac{k_{xn}}{k}D_n)\cos(k_{xn}x)\cos(k_{yn}(y-d)),\\
Z_0H_y &= \frac{j}{\epsilon_r\mu_r - 1}\sum_n (\epsilon_r\frac{k_{xn}}{k}C_n + \frac{k_{yn}}{k}D_n)\sin(k_{xn}x)\sin(k_{yn}(y-d)),
\end{aligned}
\tag{18}
$$

where $k_{xn}^2 + k_{yn}^2 = (\epsilon_r\mu_r - 1)k^2$.

From the boundary conditions at $y = b$, we obtain

$$
\begin{aligned}
(A_n + B_n)\cosh(k_{xn}b) &= C_n\sin(k_{yn}(b-d)),\\
E_{xn}^{(S)} + \frac{jk}{k_{xn}}A_n\cosh(k_{xn}b) &= \frac{j}{\epsilon_r\mu_r - 1}(\frac{k_{xn}}{k}C_n + \mu_r\frac{k_{yn}}{k}D_n)\sin(k_{yn}(b-d)),\\
E_{yn}^{(S)} + \frac{jk}{k_{xn}}B_n\sinh(k_{xn}b) &= \frac{j\epsilon_r}{\epsilon_r\mu_r - 1}(\frac{-k_{yn}}{k}C_n + \mu_r\frac{k_{xn}}{k}D_n)\cos(k_{yn}(b-d)),\\
(A_n + B_n)\sinh(k_{xn}b) &= D_n\cos(k_{yn}(b-d)),
\end{aligned}
\tag{19}
$$

where $E_{xn}^{(S)}, E_{yn}^{(S)}$ are

$$
\begin{aligned}
E_{xn}^{(S)} &= \frac{1}{a}\int_{-a}^{a} dx E_x^{(S)}(x,b)\sin(k_{xn}x),\\
E_{yn}^{(S)} &= \frac{1}{a}\int_{-a}^{a} dx E_y^{(S)}(x,b)\cos(k_{xn}x).
\end{aligned}
\tag{20}
$$

The longitudinal impedance per unit length Z/L is

$$
\begin{aligned}
\frac{Z}{L} &= -\sum_n \frac{A_n + B_n}{I_0}\\
&= \frac{j}{I_0}\sum_{n=0}^{\infty}\frac{E_{xn}^{(S)}sh + E_{yn}^{(S)}ch}{[\frac{k_{xn}}{k}(1+\epsilon_r\mu_r)sh\ ch + \frac{k_{yn}}{k}(\mu_r sh^2tn - \epsilon_r ch^2ct)]/(\epsilon_r\mu_r - 1) - \frac{k}{k_{xn}}sh\ ch}.
\end{aligned}
\tag{21}
$$

where sh, ch, tn, and ct are $\sinh(k_{xn}b), \cosh(k_{xn}b), \tan(k_{yn}(b-d))$, and $\cot(k_{yn}(b-d))$, respectively.

Equation (20) can be simplified as follows. By differentiating $E_{xn}^{(S)}$ with b, we obtain

$$
\begin{aligned}
\frac{dE_{xn}^{(S)}}{db} &= \frac{1}{a}\int_{-a}^{a} dx\frac{\partial E_x^{(S)}}{\partial y}\sin(k_{xn}x)\\
&= \frac{1}{a}\int_{-a}^{a} dx\frac{\partial E_y^{(S)}}{\partial x}\sin(k_{xn}x)\\
&= -k_{xn}\frac{1}{a}\int_{-a}^{a} dx E_y^{(S)}\cos(k_{xn}x)\\
&= -k_{xn}E_{yn}^{(S)}.
\end{aligned}
\tag{22}
$$

Similarly we obtain

$$
\frac{dE_{yn}^{(S)}}{db} = -k_{xn}E_{xn}^{(S)}.
\tag{23}
$$

These equations are solved as,

$$\begin{aligned} E_{xn}^{(S)} &= A\exp(k_{xn}b) + B\exp(-k_{xn}b), \\ E_{yn}^{(S)} &= -A\exp(k_{xn}b) + B\exp(-k_{xn}b). \end{aligned} \tag{24}$$

Since these values should go to 0 when b goes to infinity, A should be 0. So, what we have to do is to find B. This can be done by the integration of $E_y^{(S)}$ at $b = 0$.

$$\begin{aligned} B &= \lim_{b\to 0} E_{yn}^{(S)} \\ &= \frac{Z_0 I_0}{2a^2} \lim_{b\to 0} \int_{-a}^{a} dx \frac{\pi b/(2a)}{\frac{1}{2}(\pi b/a)^2 + 2\sin^2(\pi x/(2a))} \\ &= \frac{Z_0 I_0}{2a^2} \lim_{b\to 0} \frac{\pi b}{2a} \int_{-\infty}^{\infty} dx \frac{1}{\frac{1}{2}(\pi b/a)^2 + 2(\pi x/(2a))^2} \\ &= \frac{Z_0 I_0}{2a}. \end{aligned} \tag{25}$$

Thus we obtain

$$E_{xn}^{(S)} = E_{yn}^{(S)} = \frac{Z_0 I_0}{2a}\exp(-k_{xn}b). \tag{26}$$

Finally we obtain

$$\frac{Z}{L} = j\frac{Z_0}{2a}\sum_{n=0}^{\infty} \frac{1}{[\frac{k_{xn}}{k}(1+\epsilon_r\mu_r)sh\ ch + \frac{k_{yn}}{k}(\mu_r sh^2 tn - \epsilon_r ch^2 ct)]/(\epsilon_r\mu_r - 1) - \frac{k}{k_{xn}} sh\ ch}. \tag{27}$$

Figure 11 shows the longitudinal impedance per unit length. The impedance of this model at 200

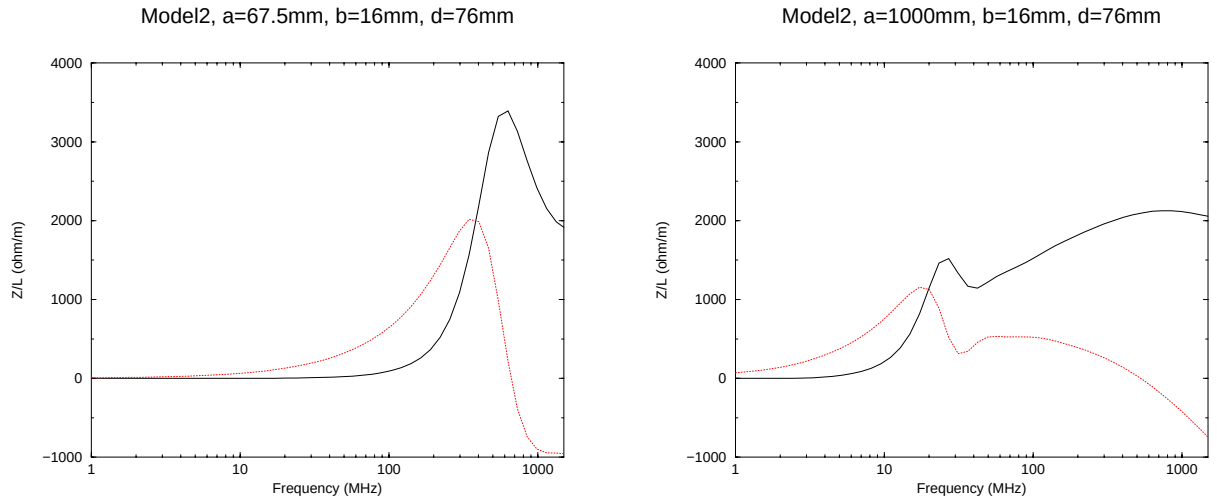

Figure 11: Longitudinal impedance per unit length for Model 2 (analytic calculation). The solid and dotted lines show the real and imaginary parts, respectively.

MHz is $Z/L = (410 + j1305)\ \Omega$/m. This value is consistent with the measurement [8]. But at higher frequencies, the real part of the impedance is 2–3 times higher than the measurement.

3.2 HFSS

The geometry is shown in Figure 12. Since this geometry is symmetric with respect to the $x = 0$ and $y = 0$ planes, we use 1/4 model to do the simulation. So we need much more volume to simulate Model

Figure 12: Model 2 geometry used for HFSS.

2 than for the Model 1. Since the number of mesh points should not exceed about 50000 due to the computer resource problem at CERN, we could not make the mesh size small enough. We used manual mesh option in HFSS so as to make the mesh size smaller than 10 mm, which is not enough. To reduce the volume, we reduced the axial length of the model from 1 m to 50 cm.

Figure 13 shows the electromagnetic field at 200MHz. The left figure shows H_ϕ at $(x, y) =$

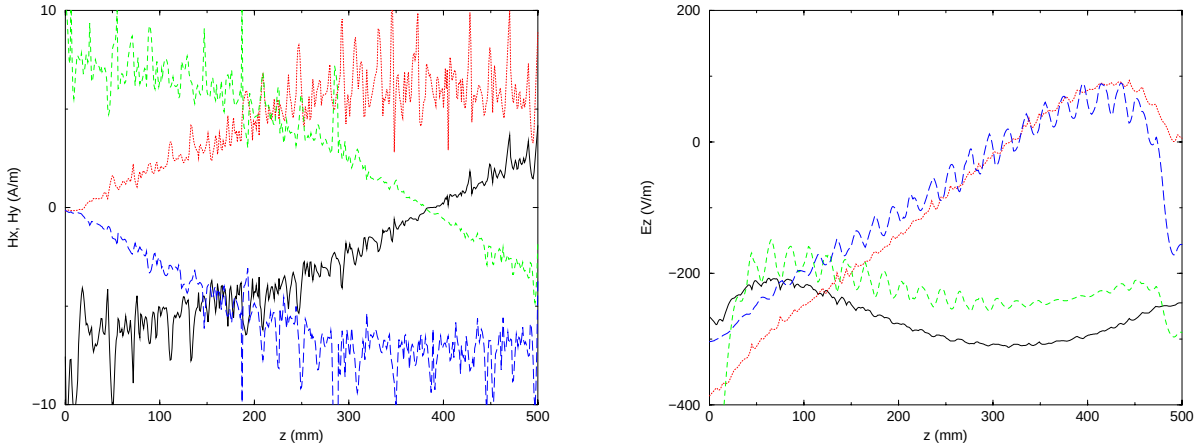

Figure 13: Electromagnetic field at 200 MHz for Model 2 by HFSS simulation. Left figure shows the transverse magnetic field at $r = 5$ mm. Solid and dotted lines are the real and imaginary parts of H_x at $(x, y) = (0, 5)$ mm, respectively. Dashed and long dashed lines are the real and imaginary parts of H_y at $(x, y) = (5, 0)$ mm, respectively. Right figure shows the axial electric field at $r = 16$ mm. Solid and dotted lines are the real and imaginary parts of E_z at $(x, y) = (0, 16)$ mm, respectively. Dashed and long dashed lines are the real and imaginary parts of E_z at $(x, y) = (16, 0)$ mm, respectively.

$(5, 0), (0, 5)$ mm, from which the current at the axis is estimated. Since the maximum value of H_ϕ is 7 A/m, The current I_0 at the axis is $I_0 \simeq 2\pi r H_\phi = 0.22$ A.

The axial component of the electric field at $(x, y) = (0, 0)$ is needed to calculate the impedance. But around the axis, the field is very noisy because the current sources are on the axis. So, the electric field at the center should be approximated using the field outside. Since the axial component of the electric field (E_z) satisfies the two dimensional Laplace equation ($\triangle_\perp E_z = 0$) in the vacuum region, one may prove the following relation:

$$E_z(r = 0) = \frac{1}{2\pi} \int_0^{2\pi} d\phi E_z(r, \phi). \tag{28}$$

We use this to estimate E_z on the axis.

The right figure shows E_z at $(x, y) = (16, 0), (0, 16)$ mm. We average these two values and obtain $E_z \simeq 280\angle -106^\circ$ V/m. Thus the impedance per unit length is $Z/L = -E_z/I_0 = (340 + j1200)\ \Omega$/m at

200 MHz by HFSS. This value is smaller than the analytical calculation by factor of 0.85. The difference between the analytical calculation and the result by HFSS may be due to the large mesh size.

Figure 14 shows the result of the HFSS simulation.

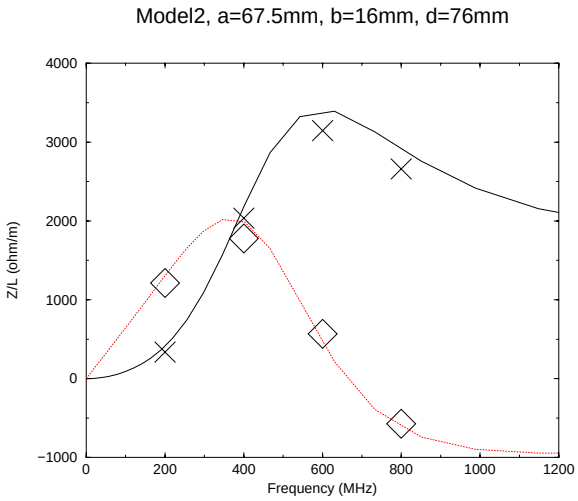

Figure 14: Longitudinal impedance per unit length of Model 2 by HFSS. Solid and dotted lines show the real and imaginary part of the impedances by analytical calculation. Cross and diamond symbols show those by HFSS simulation.

3.3 Coaxial Wire Method with HFSS

The geometry is shown in Figure 15. Input parameters for HFSS simulation are as follows. The axial

Figure 15: Model 2 geometry with wire used for HFSS.

length of the ferrite is 1 m. Two circular waveguides of 20 mm radius, 50 mm length, are added on both sides. The radius of the wire is 1 mm. The characteristic impedance Z_c of the coaxial waveguide is $Z_0/(2\pi)\log(20/1) = 180\ \Omega$. In [2], they used $Z_c = 60\log(1.27D/d)$, where D, d are the vertical aperture and the diameter of the wire. By using this, $Z_c = 181\ \Omega$, which is almost the same as our value.

From the scattering parameters, we calculate the impedance. For example at 200 MHz, we got $S_{21} = 0.43458\angle -399.225°$. We thus find

$$\begin{aligned} \mathrm{Re}(Z_{CW}/L) &= -2Z_c \log|S_{21}| = 304\ \Omega/\mathrm{m}, \\ \mathrm{Im}(Z_{CW}/L) &= -2Z_c(\arg S_{21} + \omega l/c) = 892\ \Omega/\mathrm{m}, \end{aligned}$$

where the total length l is 1.1 m. Figure 16 shows the longitudinal impedance per unit length by the coaxial wire method. We may observe that the center wire changes the resonant frequency of this system from 600 MHz to beyond 800 MHz. By comparing the result with the measurement [2], we can see that at 200 MHz, the real part of the impedance is 600 Ω by the measurement. Since the length of the ferrite in the MKE kicker is $l = 1.658$ m, the impedance by our result is 500 Ω. So, the real parts agree well. The imaginary part by the measurement is 2000 Ω. Our value is 1500 Ω. So, also, the imaginary parts agree.

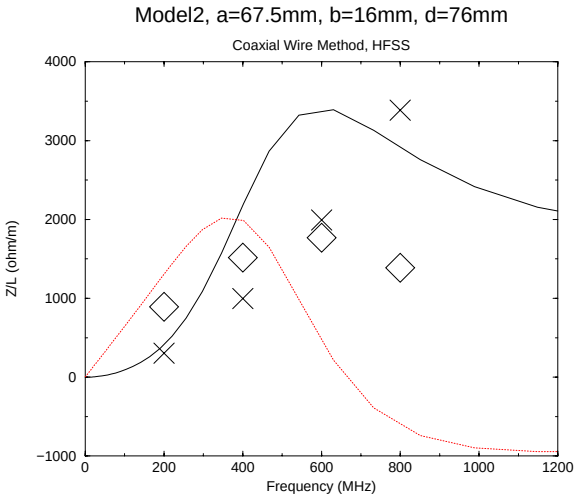

Figure 16: Longitudinal impedance per unit length for Model 2 by coaxial wire method (HFSS). Cross and diamond symbols represent the real and imaginary parts by coaxial wire method with HFSS. The solid and dotted lines show the real and imaginary parts of the impedance with beam by analytical calculation.

At 400 MHz, the real part of the impedance by the measurement is 1800 Ω, our result is 1600 Ω, so real parts agree well. But the imaginary part by the measurement is much larger than our result.

From 600 MHz, the real part of the impedance by the measurement is about twice or three times smaller than our result. The imaginary part by the measurement is much larger than our result.

4 Model 3

The discrepancy between the result of the measurement and of the HFSS simulation of Model 2 may be due to the following two reasons:

- In reality, the side plates are not like Model 2.
- The ferrite is surrounded by the vacuum vessel. Some amount of electromagnetic field travels the space between the ferrite and and vacuum vessel. This makes the impedance by the coaxial wire method small at high frequency.

To check the first point, the following model (Model 3) is studied. The model is shown in Figure 17.

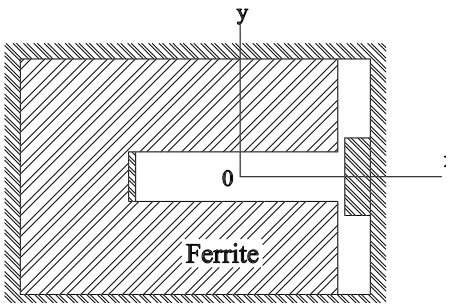

Figure 17: Model 3

Since the analytic calculation of the impedance is very complicated, we decided to do HFSS simulation only.

4.1 HFSS Simulation

The geometry is shown in Figure 18. Figure 19 shows the result of HFSS simulation. We can see the

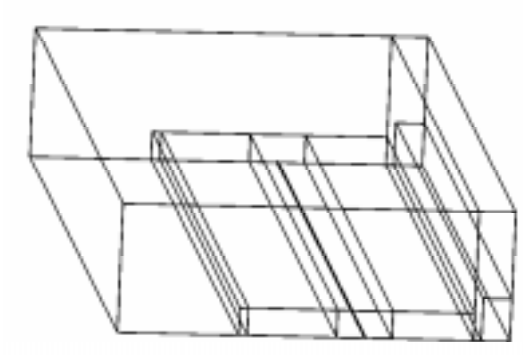

Figure 18: Model 3 geometry used for HFSS: 1/2 geometry used.

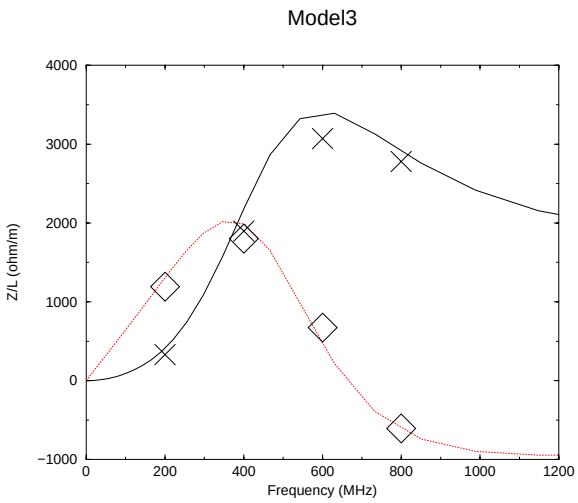

Figure 19: Longitudinal impedance per unit length of Model 3. Cross and diamond symbols show the result by HFSS simulation. Solid and dotted lines show the real and imaginary part of the impedances by analytical calculation for Model 2.

impedance is almost the same as that of Model 2.

4.2 Coaxial Wire Method with HFSS

The geometry is shown in Figure 20. We added coaxial waveguides of 20 mm radius on both sides, and calculated the scattering parameters with HFSS. The radius of the wire is 1 mm. Since the geometry is symmetric with respect to the $y = 0$ plane, we used 1/2 geometry.

From the scattering parameters, we calculate the impedance. For example at 200 MHz, we got $S_{21} = 0.47126\angle - 397.312°$. Thus we find

$$\begin{aligned} \mathrm{Re}(Z_{CW}/L) &= -2Z_c \log|S_{21}| = 286\ \Omega/\mathrm{m}, \\ \mathrm{Im}(Z_{CW}/L) &= -2Z_c(arg S_{21} + \omega l/c) = 883\ \Omega/\mathrm{m}, \end{aligned}$$

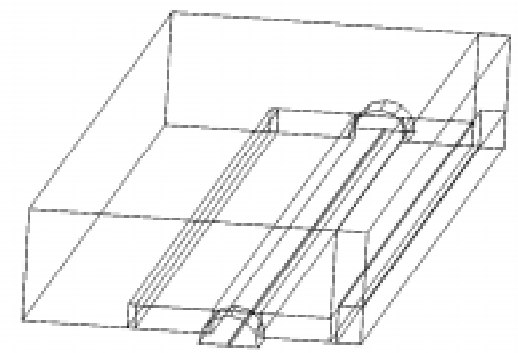

Figure 20: Model 3 geometry with wire used for HFSS.

where the total length l is 1.1 m. Figure 21 shows the longitudinal impedance per unit length by the coaxial wire method. At high frequencies, the imaginary part becomes larger than that for the Model 2.

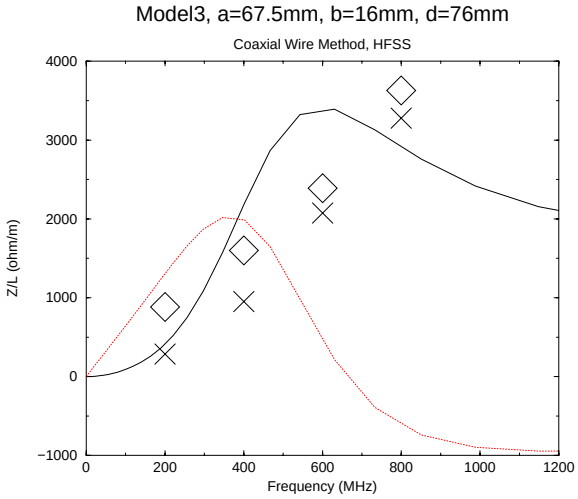

Figure 21: Longitudinal impedance per unit length for Model 3 by coaxial wire method (HFSS). Cross and diamond symbols represent the real and imaginary parts by coaxial wire method with HFSS. The solid and dotted lines show the real and imaginary parts of the impedance with beam by analytical calculation for Model 2.

This may be due to a trapped mode around the outer metal plate.

5 Model 4

Since Model 2 or Model 3 did not reproduce the measurement by the coaxial wire method, there must be some other reasons.

Since there are spaces between the ferrite block and the vacuum vessel, electromagnetic field at high frequency can go through these spaces easily. If the attenuation constants γ of these waveguides are very small, the fields go through these waveguides without attenuation and are gathered at the exit of the kicker. This makes $\mathrm{Re}(Z_{CW})$ lower. The imaginary part $\mathrm{Im}(Z_{CW})$ may become larger, because such waveguides give the inductive impedance. These waveguides make resonances and the behavior of the impedance as a function of frequency very complicated.

To see the effect of this, we input an almost realistic geometry to HFSS and simulated the coaxial wire method. The total length of the ferrite is too long (1.658 m) to do the real beam simulation with HFSS.

5.1 Coaxial Wire Method with HFSS

The geometry is shown in Figure 22. Figure 23 shows the longitudinal impedance by the coaxial wire

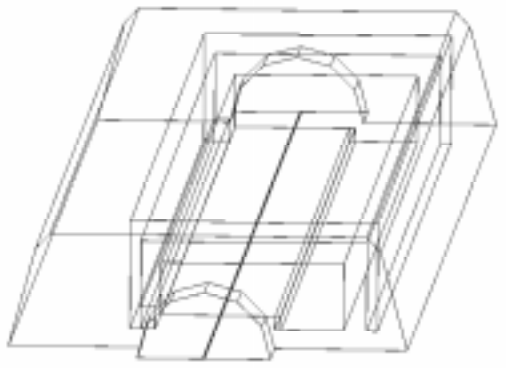

Figure 22: Model 4 geometry with wire used for HFSS.

method.

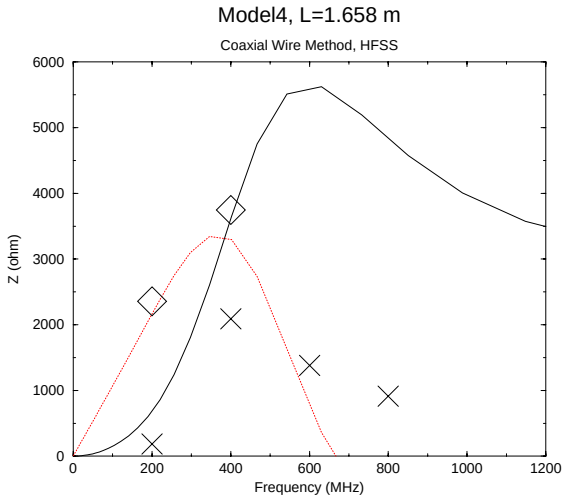

Figure 23: Longitudinal impedance for Model 4 by coaxial wire method (HFSS). Cross and diamond symbols represent the real and imaginary parts by coaxial wire method with HFSS. The solid and dotted lines show the real and imaginary parts of the impedance with beam by analytical calculation for Model 2.

Since this model has a big volume, the result has large errors.

There is some ambiguity on the determination of Z_c. At both ends, the radius of the beamduct is 76 mm. Thus, the characteristic impedance Z_c is 260 Ω. The result by HFSS is 270 Ω. In this figure, we used $Z_c = 270\ \Omega$. But in the ferrite region Z_c should be 180 Ω. So, there is the ambiguity of factor of 1.5.

At 200 MHz, the real part of Z_{CW} is 190 Ω, which is much smaller than the measurement. There are some resonances from 400 MHz. They may reduce the real part of the impedance at higher frequencies.

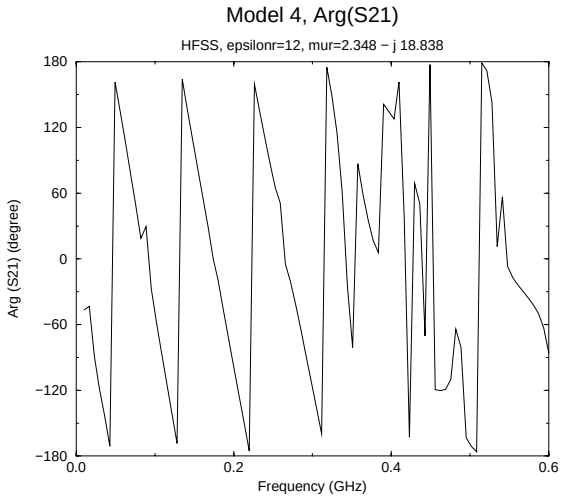

Figure 24: Argument of S_{21} for Model 4 coaxial wire method by HFSS simulation. The relative permeability is 2.348 - j 18.838 for whole frequency range. Resonances can be seen from 400 MHz.

n	Frequency (GHz)	$\lvert I_n/I_0\rvert$	Re$(Z)(\Omega)$	
			Model 1	Model 2
0	0.0	1.0	0	0
1	0.2	0.915	7090	680
2	0.4	0.63	4820	3611
3	0.6	0.41	3842	5664
4	0.8	0.24	3280	4961
5	1.0	0.1	2918	3971

Table 1: Some parameters for power calculation of the SPS MKE kicker.

The resonances can be easily seen in Figure 24. For each frequency, we plot this kind of figure to determine $\arg S_{21}$. This figure is with the parameters at 600 MHz. We can see that from 350 MHz, there are some resonances. They change the phase of S_{21}. Because of the resonances, we cannot determine the phase at 600 MHz and 800 MHz. Model 4 seems to have smaller Re(Z_{CW}) beyond 600 MHz than Model 3. This shows the effect of by-passing electromagnetic field.

Figure 25 shows the electric field on $y = 0$ plane at 600 MHz.

6 Estimation of the Power

The power dissipated in the kicker can be calculated with the following equation:

$$P = \sum_{n=-\infty}^{\infty} \text{Re}(Z(n\omega_0))|I_n|^2, \tag{29}$$

where ω_0 is the angular frequency of the ring ($2\pi/T_0$). The n-th fourier component I_n of the current I_0 is $< I_0 \exp(-jn\omega_0 t) >$.

We apply this formula to the SPS MKE kicker. There was a measurement at I_0 = 0.134 A. The measured power is 60 W [9]. The fourier components of the current and the impedances of Model 1 and Model 2 are shown in Table 1.

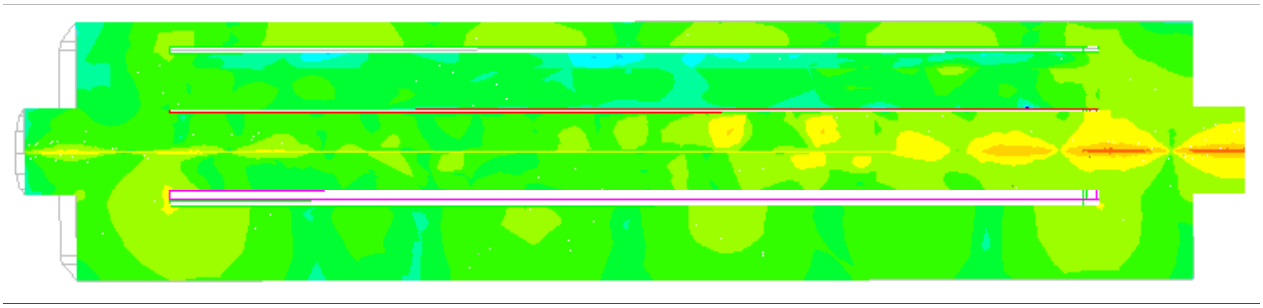

Figure 25: Electric field on the y = 0 plane at 600 MHz. Waves go from right to left. Waves around the wire attenuate quickly, and disappears at a certain distance. Some waves are transmitted via the space between ferrite and vacuum vessel, and joined at the exit of the kicker.

The power is

$$P = \eta |I_0|^2 \sum_{n=-5}^{5} |I_n/I_0|^2 \mathrm{Re}(Z(n\omega_0)) = \begin{cases} 78\ W, & \text{Model 1} \\ 29\ W, & \text{Model 2} \end{cases} \tag{30}$$

where we multiply by the efficiency $\eta = 0.25$, since the beam is present for 1/4 of the whole cycle. They agree with the measurement within a factor of two.

7 Conclusion

Both Model 1 and Model 2 give reasonable power dissipation. Model 2 seems to be more realistic. The coaxial wire method tends to give lower real part of the longitudinal coupling impedance.

Acknowledgment

I would like to thank D. Brandt, L. Vos, A. Mostacci, F. Caspers, M. Dyachkov, and E. Shaposhnikova for valuable discussions. I would like to thank F. Ruggiero for correcting English. I would like to thank E. Jensen and T. M. Lopez for information of Ansoft HFSS.

References

[1] L. Vos, “Longitudinal Impedance from Ferrite”, CERN SL/Note (AP), to be published (2000)

[2] F. Caspers and M. D’yachkov, “Measurement Done with a Single Wire on the SPS MKE Kicker”, CERN-LHC-Project-Report, to be published (2000).

[3] http://www.ansoft.com

[4] A. W. Chao, “Physics of Collective Beam Instabilities in High Energy Accelerators”, Wiley, New York, (1993).

[5] W. Hartung et al., “Assessment of the Coupling Impedance of Beam Line Higher-Order Mode Loads”, in Proceedings of the Workshop on Microwave-Absorbing Materials for Accelerators (1993).

[6] Soft Ferrites, Philips Components (1990).

[7] F. Caspers et al., “Measurements of Complex Permeability and Permittivity of Ferrites for the LHC Injection Kicker”, CERN-LHC-Project-Note 203 (1999).

[8] F. Caspers et al., “RF Screening by Thin Resistive Layers”, CERN-LHC-Project-Report-300 (1999).

[9] F. Caspers, private communication.